Supporting Information

Realizing Efficient Broadband Near-Infrared Emission under Blue Light Excitation in Sb^{3+}-Doped Zero-Dimensional Organic Tin(IV)-Based Metal Halides via Coordination Structure Modulation

Bao Ke,[†] Hui Peng[‡,]*, Yongqi Yang,[†] Chengzhi Yang,[†] Shangfei Yao,[†] Arfan Bukhtiar,[†] Qilin Wei,[§,]* Jialong Zhao[†,‡] Bingsuo Zou[†,‡]*

* Corresponding Authors

[†]School of Physical Science and Technology, Guangxi University, Nanning 530004, China.

[‡]State Key Laboratory of Featured Metal Materials and Life-cycle Safety for Composite Structures, and School of Resources, Environment and Materials, Guangxi University, Nanning 530004, China.

[§]School of Chemistry and Chemical Engineering, Shandong University, Jinan 250100, China.

E-mail: penghuimaterial@163.com (H. Peng); qlwei@sdu.edu.cn (Q. Wei); zoubs@gxu.edu.cn (B. Zou).

Table S1. Single crystal X-ray diffraction data of $(TBP)_2SnBr_6$ and $(TBP)_2SbBr_5$.

Empirical formula	$(TBP)_2SnBr_6$	$(TBP)_2SbBr_5$
Chemical formula	$C_{32}H_{72}Br_6P_2Sn$	$C_{32}H_{71}Br_5P_2Sb$
Formula weight	1116.98	1039.12
Temperature (K)	296.15	193
Crystal system	monoclinic	triclinic
Space group	C2/c	P-1
a (Å)	14.669(4)	11.756(4)
b (Å)	18.782(5)	11.880(4)
c (Å)	18.250(7)	16.979(5)
α (deg)	90	98.786(8)
β (deg)	113.585(5)	96..418(9)
γ (deg)	90	104.761(8)
Volume (Å^3)	4608(2)	2237.9(12)
Z	4	2
Density (calculated) (g·cm^{-3})	1.610	1.5442
Absorption coefficient (mm^{-1})	5.846	5.170
Index ranges	$-17 \le h \le 17$, $-14 \le k \le 22$, $-21 \le l \le 20$	$-15 \le h \le 15$, $-14 \le k \le 15$, $-22 \le l \le 19$
Independent reflections	4058 [R_{int} = 0.0736, R_{sigma} = 0.0845]	10314 [R_{int} = 0.0511, R_{sigma} = 0.0948]
Data/restraints/parameters	4058/2/191	10314/0/369
Goodness of fit on F^2	1.050	1.023
Final R indexes [I>=2σ (I)]	R_1 = 0.0577, wR_2 = 0.1332	R_1 = 0.0538, wR_2 = 0.0996
Final R indexes [all data]	R_1 = 0.1003, wR_2 = 0.1537	R_1 = 0.1210, wR_2 = 0.1241
Largest diff. peak and hole (eÅ^{-3})	0.73 and -1.26	0.85 and -1.09

Table S2. Bond angles of $(TBP)_2SnBr_6$ and $(TBP)_2SbBr_5$ SCs.

Samples	Atom	Atom	Atom	Angle/°
$(TBP)_2SnBr_6$	Br2	Sn1	Br1	180
	Br3[1]	Sn1	Br1	88.74(2)
	Br3	Sn1	Br1	88.74(2)
	Br3	Sn1	Br2	91.26(2)
	Br3[1]	Sn1	Br2	91.26(2)
	Br3	Sn1	Br3[1]	177.48(4)
	Br4[1]	Sn1	Br1	89.77(2)
	Br4	Sn1	Br1	89.77(2)
	Br4	Sn1	Br2	90.23(2)
	Br4[1]	Sn1	Br2	90.23(2)
	Br4[1]	Sn1	Br3	89.35(4)
	Br4[1]	Sn1	Br3[1]	90.64(4)
	Br4	Sn1	Br3	90.64(4)
	Br4	Sn1	Br3[1]	89.35(4)
	Br4	Sn1	Br4[1]	179.53(4)
$(TBP)_2SbBr_5$	Br(2)	Sb(1)	Br(1)	87.85(3)
	Br(2)	Sb(1)	Br(4)	179.57(3)
	Br(2)	Sb(1)	Br(3)	88.71(3)
	Br(4)	Sb(1)	Br(1)	92.28(3)
	Br(4)	Sb(1)	Br(3)	91.16(3)
	Br(5)	Sb(1)	Br(1)	90.45(3)
	Br(5)	Sb(1)	Br(2)	90.87(4)
	Br(5)	Sb(1)	Br(4)	88.71(3)
	Br(5)	Sb(1)	Br(3)	89.84(3)
	Br(3)	Sb(1)	Br(1)	176.55(3)

Table S3. Bond lengths of $(TBP)_2SnBr_6$ and $(TBP)_2SbBr_5$ SCs.

$(TBP)_2SnBr_6$			$(TBP)_2SbBr_5$		
Atom	Atom	Length/Å	Atom	Atom	Length/Å
Sn1	Br1	2.6272(14)	Sb(1)	Br(1)	2.7794(10)
Sn1	Br2	2.6043(14)	Sb(1)	Br(2)	2.7503(10)
Sn1	Br3	2.5932(10)	Sb(1)	Br(3)	2.7761(10)
Sn1	Br4	2.5932(10)	Sb(1)	Br(4)	2.5172(10)
Sn1	Br5	2.5869(12)	Sb(1)	Br(5)	2.7770(10)
Sn1	Br6	2.5868(12)	-	-	-

Table S4. Elemental compositions of samples obtained from EDS analysis of Sb^{3+}: $(TBP)_2SnBr_6$.

element	5%	10%	15%	20%
Br	85.5	86.97	85.54	72.98
Sb	0.35	0.98	2.1	5.36
Sn	14.15	12.05	12.35	21.66
Sb/(Sn+Sb) %	2.41	7.52	14.53	19.84

Table S5. Optical parameters of antimony induced with NIR emission in metal halides.

Compounds	PLE (nm)	PL (nm)	PLQY (%)	Ref.
Sb^{3+}:Cs_2ZnCl_4	316	745	69.9	1
Sb^{3+}:Cs_2ZnBr_4	368	823	< 20	
Sb^{3+}:$Cs_2SnCl_4Br_2$	410	710	8	2
Sb^{3+}:$Rb_2InBr_5 \cdot H_2O$	365	750	20	3
Sb^{3+}: $(NH_4)_2SnCl_6$	360	734	23	4
$(C_{13}H_{22}N)_2Sb_2Cl_8$	350	865	5	
$(C_{10}H_{16}N)_2Sb_2Cl_8$	345	990	3	5
$(C_{16}H_{36}P)SbCl_4$	335	1070	1	
$(C_{19}H_{18}P)_2SbBr_5$ glass	450	735	5.5	6
dis-TPP_2SbBr_5	400	738	3.3	7
Sb^{3+}: $(TBP)_2SnBr_6$	452	705	33.22	This work

Table S6. The degree of $(TBP)_2SbBr_5$, Sb^{3+}:$(TBP)_2SnBr_6$ and Sb^{3+}:$(TBP)_2SnCl_6$ configuration distortions.

Compounds	σ^2	Δd
$(TBP)_2SbBr_5$	2.21	$1.4*10^{-3}$
Sb^{3+}:$(TBP)_2SnBr_6$	0.75	$2.92*10^{-5}$
Sb^{3+}:$(TBP)_2SnCl_6$*	0.62	$2.17*10^{-5}$

*Data from *Adv. Optical Mater*. 2023, 2301665.

Table S7. Comparison of the bond lengths of $(TBP)_2SbBr_5$, undoped and Sb^{3+}-doped $(TBP)_2SnBr_6$ samples in the ground state and excited state.

$(TBP)_2SbBr_5$

	Sb-Br1 (Å)	Sb-Br2 (Å)	Sb-Br3 (Å)	Sb-Br4 (Å)	Sb-Br5 (Å)	Δd
Ground state	2.7945	2.5832	2.807	2.8295	2.7831	$1.05*10^{-3}$
Excited state	3.3862	3.7946	3.4719	3.8229	3.4305	$2.75*10^{-3}$

$(TBP)_2SnBr_6$

	Sb-Br1 (Å)	Sb-Br2 (Å)	Sb-Br3 (Å)	Sb-Br4 (Å)	Sb-Br5 (Å)	Sb-Br6 (Å)	Δd
Ground state	2.7087	2.7245	2.7055	2.7292	2.7055	2.7087	$1.23*10^{-5}$
Excited state	3.3897	3.4255	3.389	3.4424	3.4256	3.3897	$4.01*10^{-5}$

Sb^{3+}:$(TBP)_2SnBr_6$

	Sb-Br1 (Å)	Sb-Br2 (Å)	Sb-Br3 (Å)	Sb-Br4 (Å)	Sb-Br5 (Å)	Sb-Br6 (Å)	Δd
Ground state	2.7087	2.7245	2.7055	2.7292	2.7055	2.7087	$1.23*10^{-5}$
Excited state	3.3339	3.3555	3.3178	3.3774	3.3558	3.3173	$4.30*10^{-5}$

Evaluation of metal halide configuration distortion:

The degree of metal halide configuration distortions is assessed using the distortion parameters (Δd) and the magnitude of asymmetric coordination environment (σ^2) of [Sn(Sb)Br_6] and [$SbBr_5$] units, and their values can be determined using the following equations:

Sb^{3+}-doped $(TBP)_2SnBr_6$ SCs:

$$\sigma^2 = \left(\frac{1}{11}\right)\sum_{i=1}^{12}(\theta_i - 90°)^2 \quad (1)$$

$$\Delta d = \left(\frac{1}{6}\right)\sum_{n=1}^{6}\left[\frac{d_n - d_{ave}}{d_{ave}}\right]^2 \quad (2)$$

$(TBP)_2SbBr_5$ SCs:

$$\sigma^2 = \left(\frac{1}{7}\right)\sum_{i=1}^{8}(\theta_i - 90°)^2 \quad (3)$$

$$\Delta d = \left(\frac{1}{5}\right)\sum_{n=1}^{5}\left[\frac{d_n - d_{ave}}{d_{ave}}\right]^2 \quad (4)$$

where θ_i represents the angle of Br-Sn(Sb)-Br, $d_n$is the distances of Sn(Sb)-Br bonds, and d_{ave}

denotes the average Sn(Sb)-Br bond length.

The lattice deformation parameters (Δd) in the ground state and excited state for Sb(III)-based compound and Sb^{3+}-doped samples were also given in Table S7. Moreover, the excited state lattice distortion degree (η) was calculated via the following equation (5):

$$\eta = \frac{\Delta d_{ES} - \Delta d_{GS}}{\Delta d_{GS}} \times 100\% \quad (5)$$

where Δd_{GS} and Δd_{ES} are the lattice deformation parameters (Δd) in the ground state and excited state, respectively. Here, the calculated η of $(TBP)_2SbBr_5$, $(TBP)_2SnBr_6$ and Sb^{3+}:$(TBP)_2SnBr_6$ are 161.8%, 227.3% and 250.8%, respectively. Clearly, the values of η for the Sb^{3+}-doped $(TBP)_2SnBr_6$ is much larger than Sb(III)-based compound, resulting in a larger Stokes shift in Sb^{3+}-doped samples and further enabling us to obtain NIR emission.

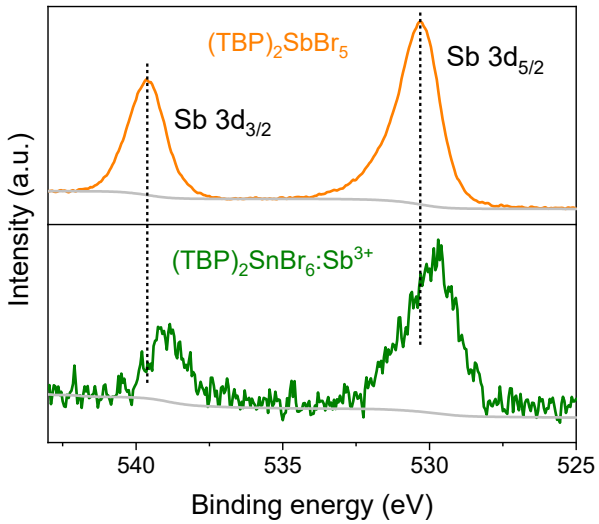

Figure S1. HRXPS spectra of Sb 3d for $(TBP)_2SbBr_5$ and $0.15Sb^{3+}$-doped $(TBP)_2SnBr_6$.

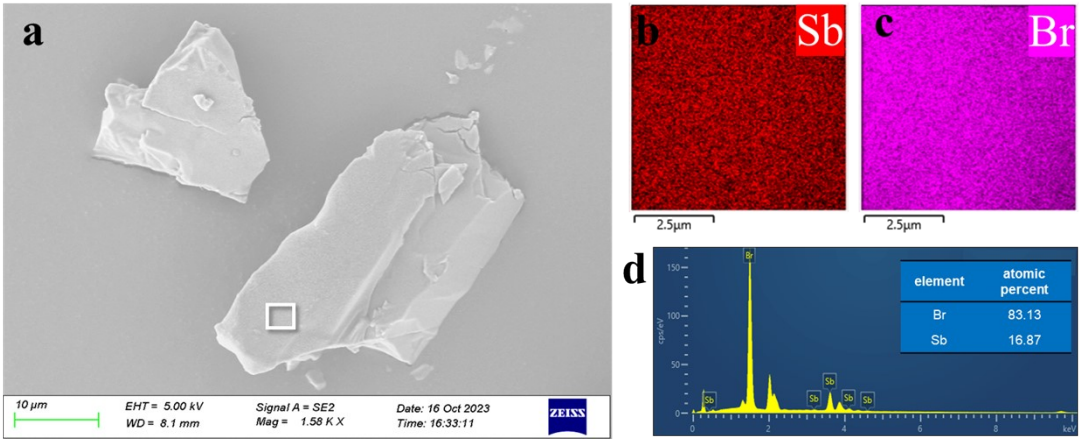

Figure S2. SEM (a), EDS element mapping (b, c) and EDS spectrum (d) of $(TBP)_2SbBr_5$ samples.

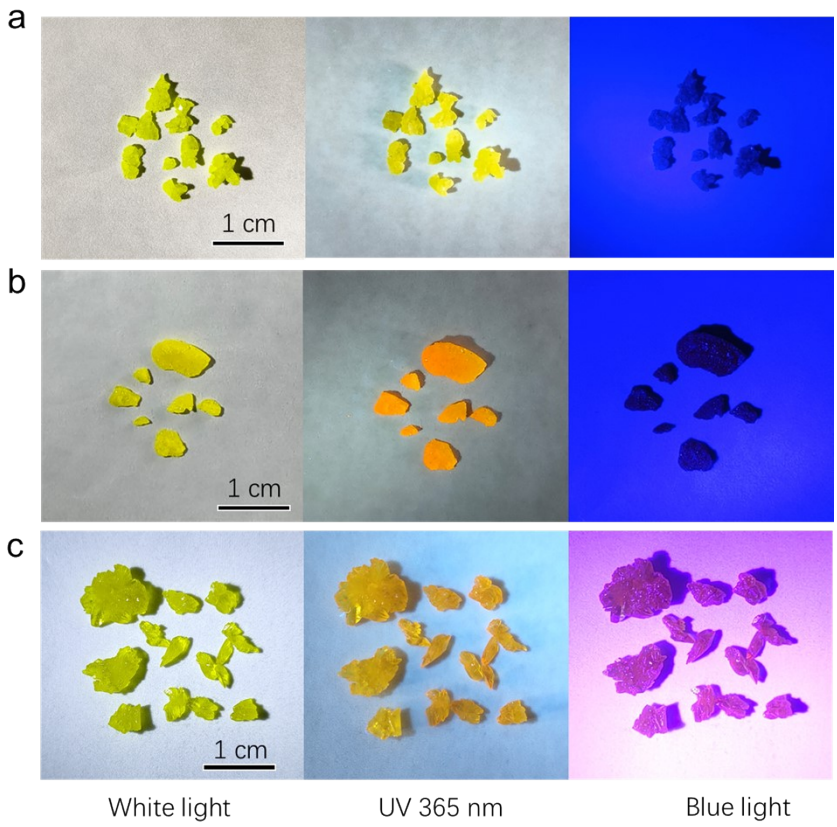

Figure S3. Optical images of (a) $(TBP)_2SnBr_6$ (b) $(TBP)_2SbBr_5$ and (c) $0.15Sb^{3+}$-doped $(TBP)_2SnBr_6$ SCs.

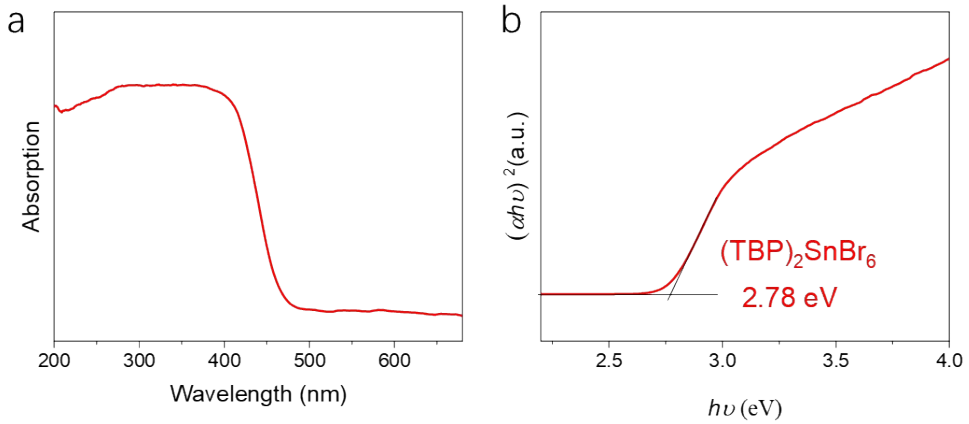

Figure S4. UV-vis absorption spectra of $(TBP)_2SnBr_6$ (a) and the corresponding Tauc plot (b).

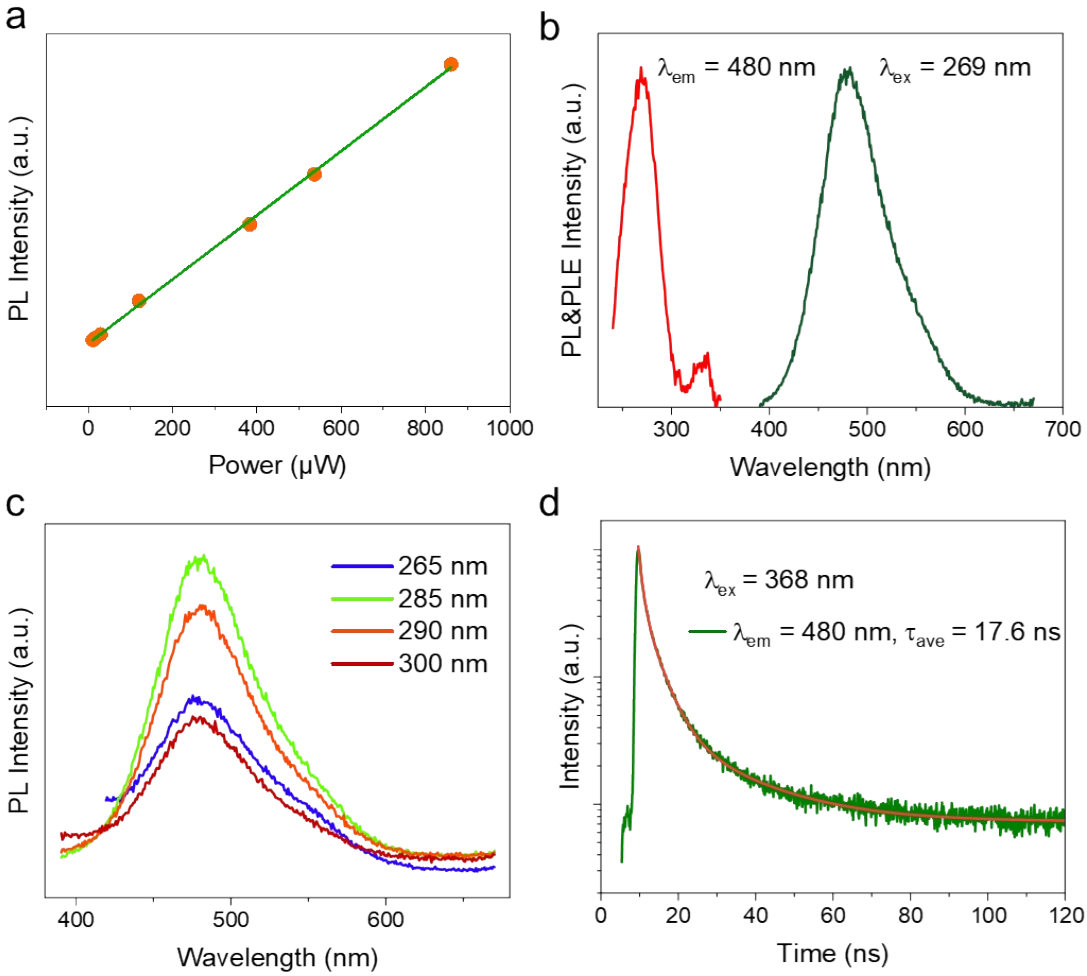

Figure S5. (a) Fitting results of PL intensity versus excitation power for $(TBP)_2SnBr_6$. (b) PL and PLE spectra of $(TBP)_2SnBr_6$ at RT. (c) PL spectra of $(TBP)_2SnBr_6$ recorded using different excitation wavelength at RT. (d) PL decay lifetime of $(TBP)_2SnBr_6$ monitoring at different emission wavelengths at RT.

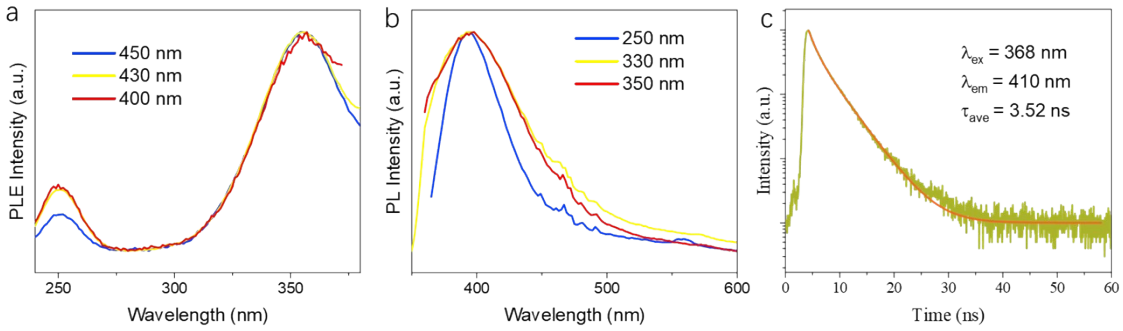

Figure S6. (a) PLE of TBPBr monitoring at different emission wavelengths at RT. (b) PL of TBPBr monitoring at different excitation wavelengths at RT. (c) PL decay curves of TBPBr at RT.

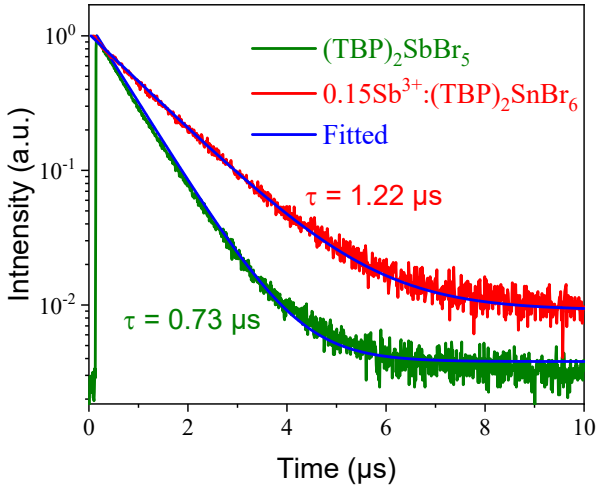

Figure S7. PL decay curves were obtained for $(TBP)_2SbBr_5$ and $0.15Sb^{3+}$-doped $(TBP)_2SnBr_6$ under 405 nm excitation at RT.

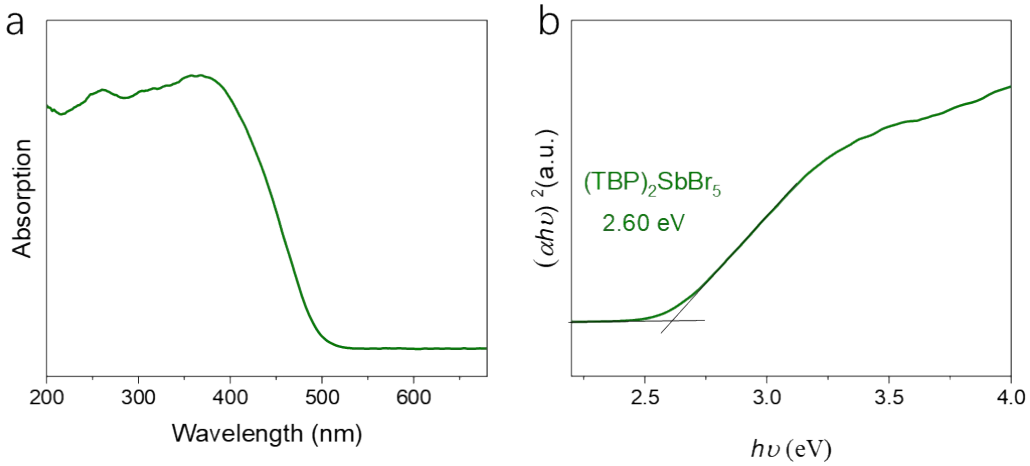

Figure S8. UV-vis absorption spectra of $(TBP)_2SbBr_5$ (a) and the corresponding Tauc plot (b).

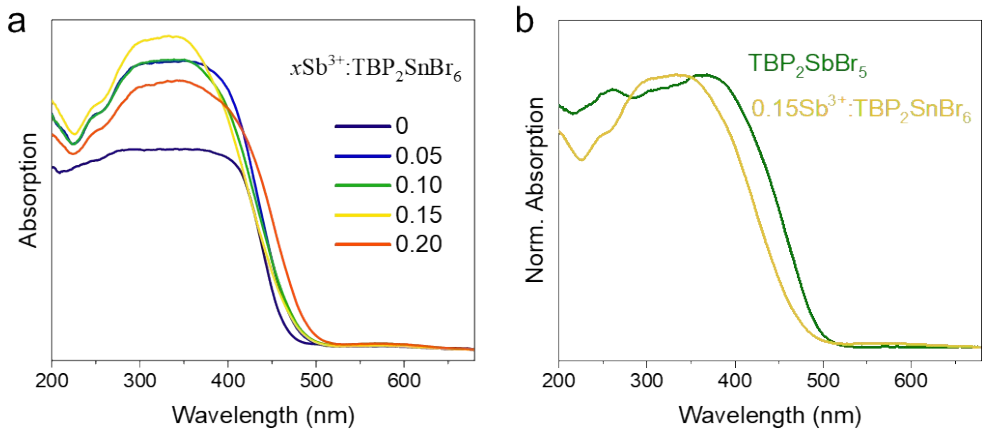

Figure S9. (a) UV-vis absorption spectra of Sb^{3+}-doped $(TBP)_2SnBr_6$ with various Sb/(Sn+Sb) ratios. (b) UV-vis absorption spectra of $(TBP)_2SbBr_5$ and $0.15Sb^{3+}$-doped $(TBP)_2SnBr_6$.

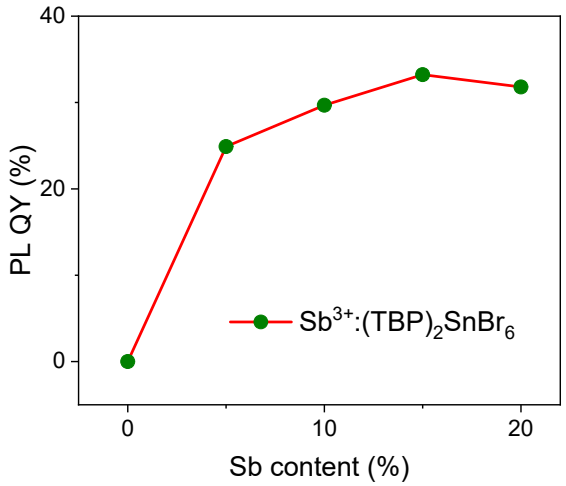

Figure S10. PLQY of Sb^{3+}-doped $(TBP)_2SnBr_6$ SCs with various Sb/(Sn+Sb) ratios.

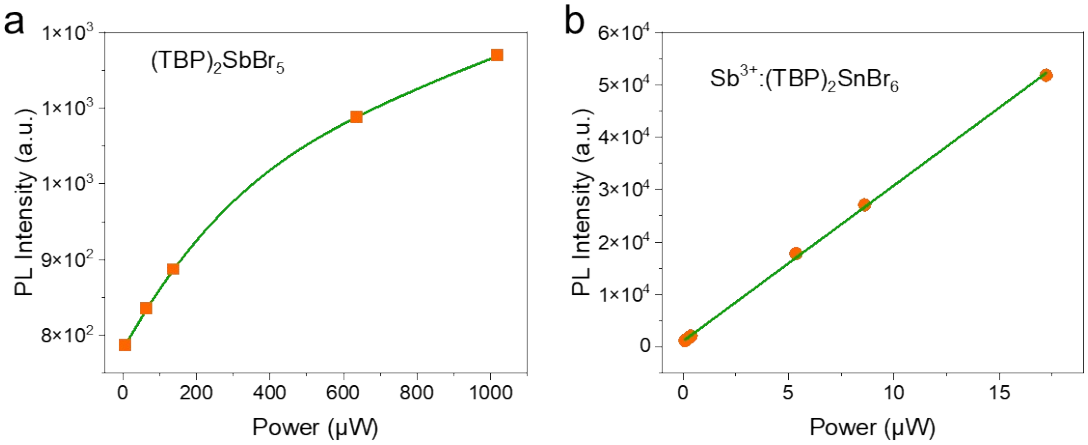

Figure S11. Fitting results of PL intensity versus excitation power for $(TBP)_2SbBr_5$ (a) and Sb^{3+}-doped $(TBP)_2SnBr_6$ (b).

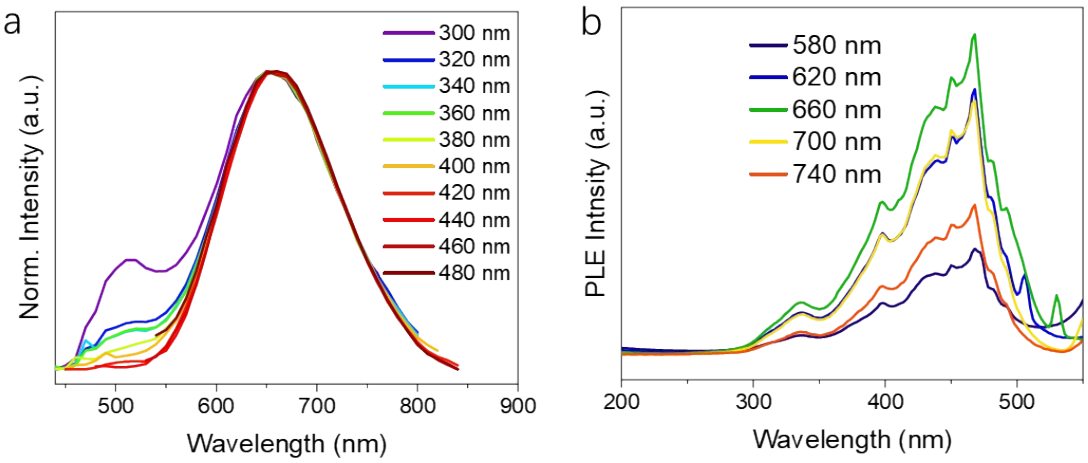

Figure S12. The optical properties of $(TBP)_2SbBr_5$: (a) PL spectra recorded using different excitation wavelength at RT. (b) PLE spectra recorded using different emission wavelength at RT.

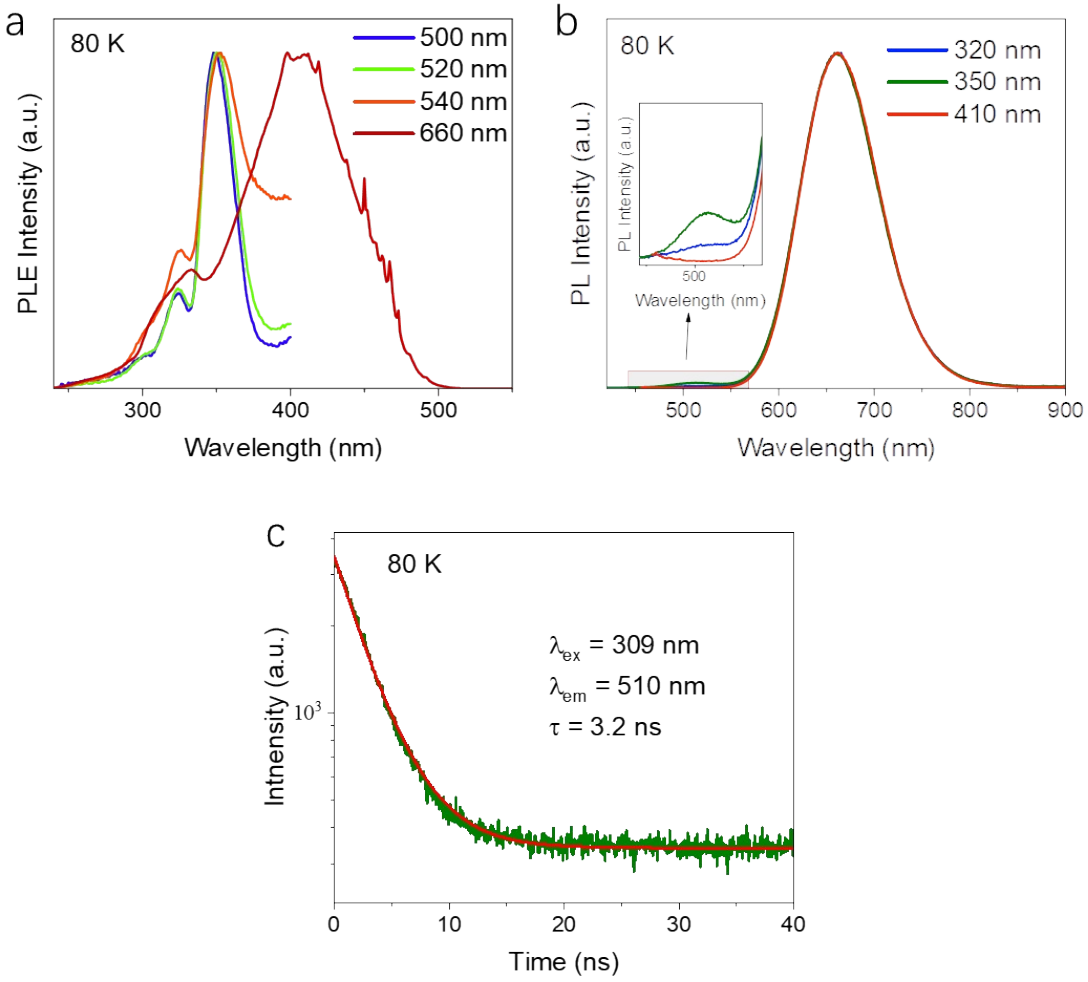

Figure S13. The optical properties of $(TBP)_2SbBr_5$: (a) PLE spectra recorded using different emission wavelength at 80K. (b) PL spectra recorded using different excitation wavelength at 80 K. (c) PL decay lifetime at 80 K.

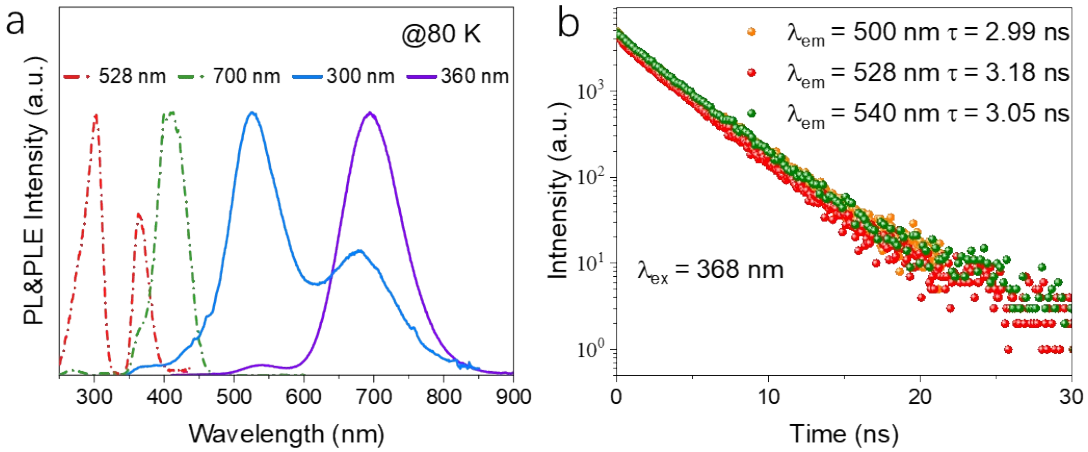

Figure S14. (a) Normalized PL and PLE spectra and (b) PL decay lifetime of Sb^{3+}-doped $(TBP)_2SnBr_6$ SCs at 80 K.

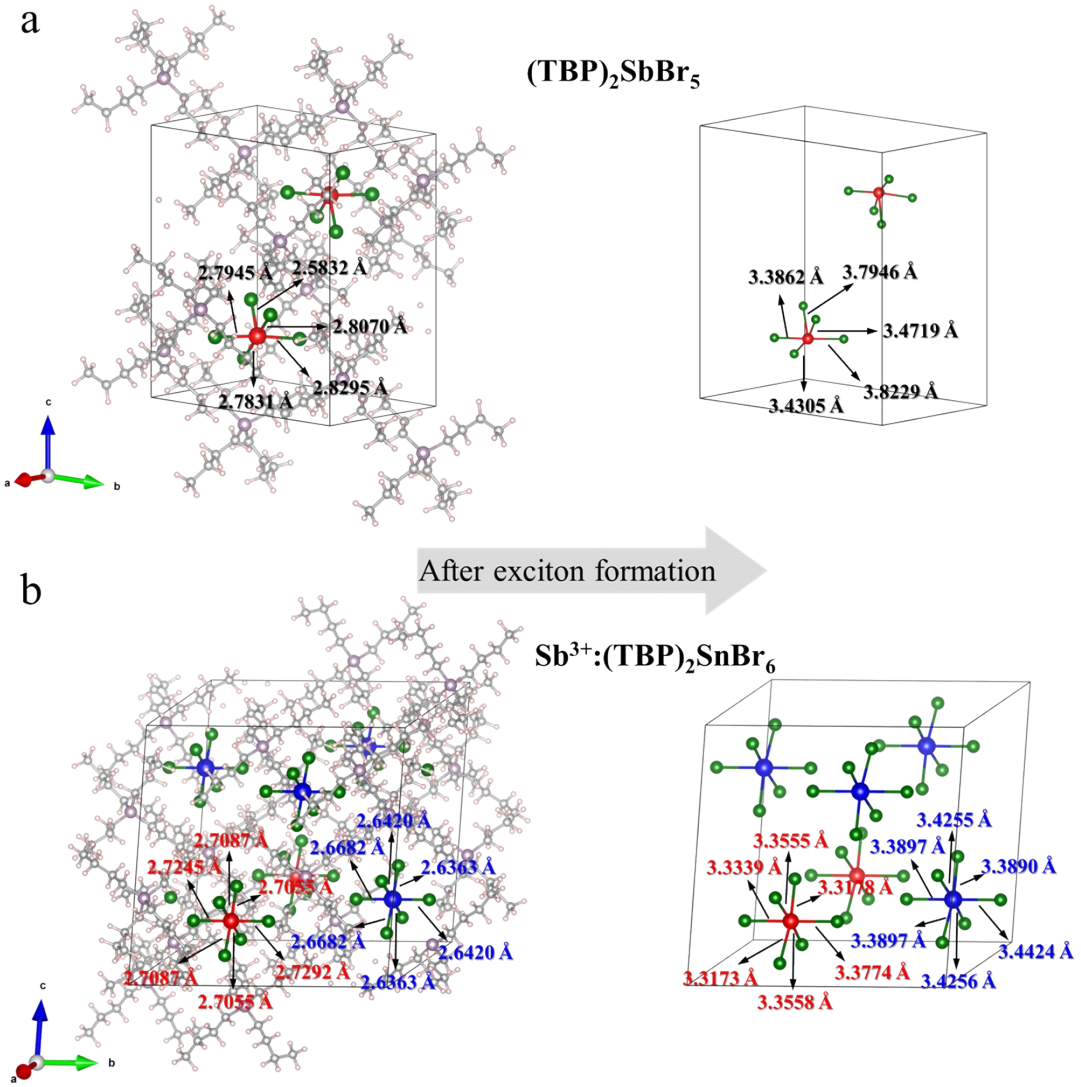

Figure S15. (a) The Sb-Br bond lengths of square-pyramidal $[SbBr_5]^{2-}$ for $(TBP)_2SbBr_5$ in the ground state (left) and excited state (right). (b) The Sn/Sb-Br bond lengths of octahedron-shaped $[Sn/SbBr_6]$ for Sb^{3+}-doped $(TBP)_2SnBr_6$ in the ground state (left) and excited state (right).

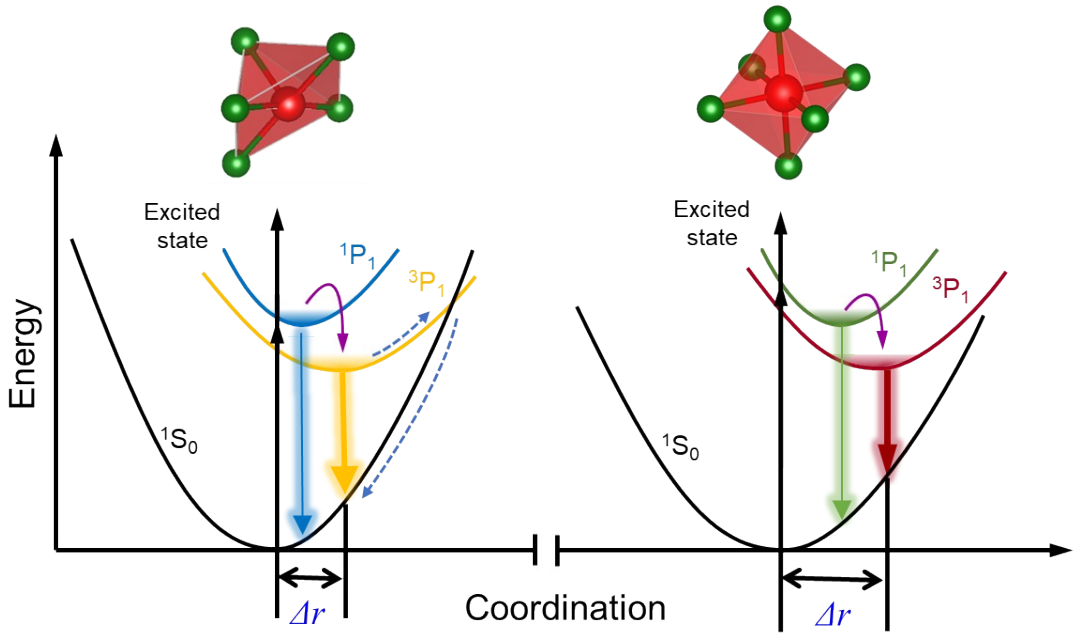

Figure S16. Structures of the metal halide polyhedrons and the corresponding configuration–coordinate diagrams of the ns^2 metal ions. (a) $[SbBr_5]^{2-}$ polyhedron with large distortion is favorable for the low PL intensity of the $(TBP)_2SbBr_5$; (b) $[SbBr_6]^{3-}$ clusters with small distortion is favorable for the high PL intensity of the Sb^{3+}-doped $(TBP)_2SnBr_6$. The lattice distortion degree enables Sb^{3+}-doped $(TBP)_2SnBr_6$ exhibits a large Stokes shift and yield a broadband NIR emission. Blue dotted line: energy dissipation and loss; Δr: Stokes shift.

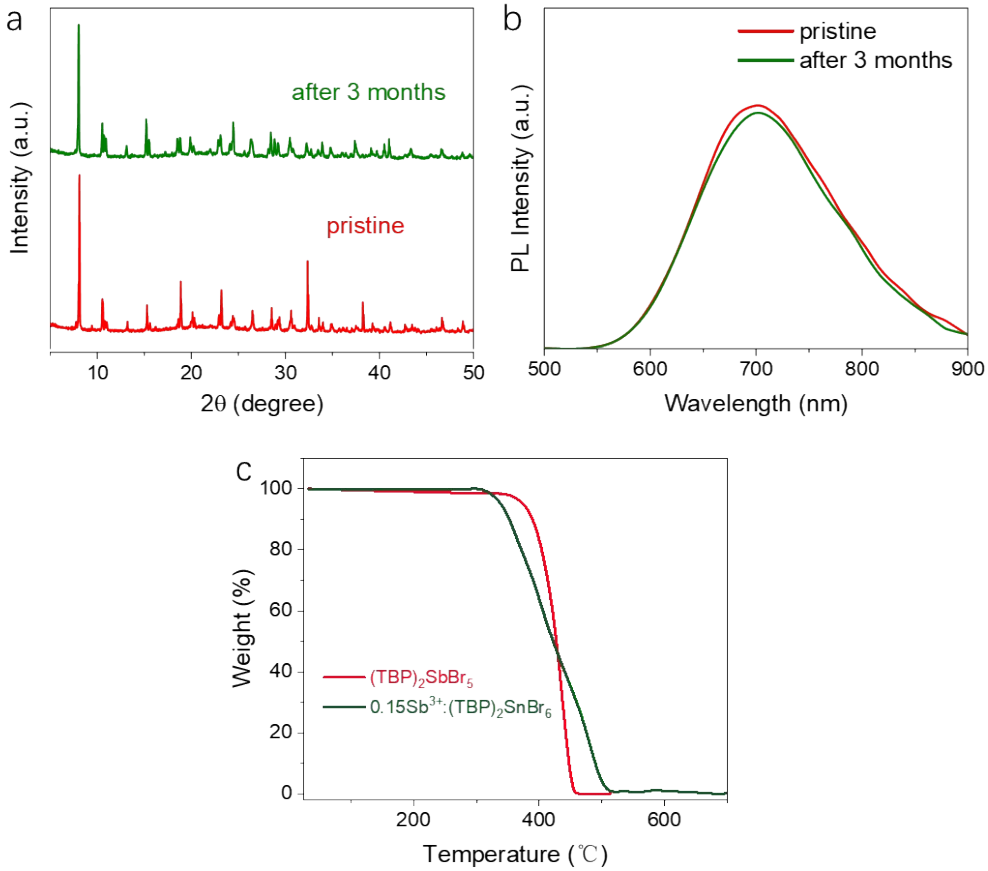

Figure S17. (a) PXRD patterns of Sb^{3+}-doped $(TBP)_2SnBr_6$ stored in atmospheric environment for 3 months. (b) Normalized PL spectra of Sb^{3+}-doped $(TBP)_2SnBr_6$ stored in atmospheric environment for 3 months. (c) TG curves of $(TBP)_2SbBr_5$ and Sb^{3+}-doped $(TBP)_2SnBr_6$ powders.

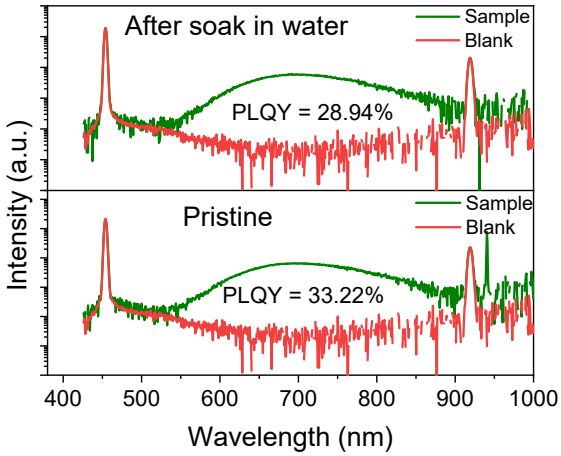

Figure S18. The change of Sb^{3+}-doped $(TBP)_2SnBr_6$ in PLQY before and after immersion in water for 4 h.

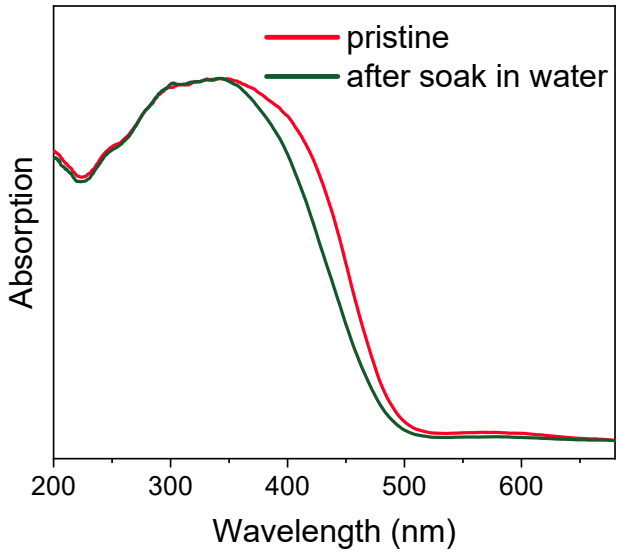

Figure S19. Absorption spectra of pristine and after soak in water for Sb^{3+}-doped $(TBP)_2SnBr_6$.

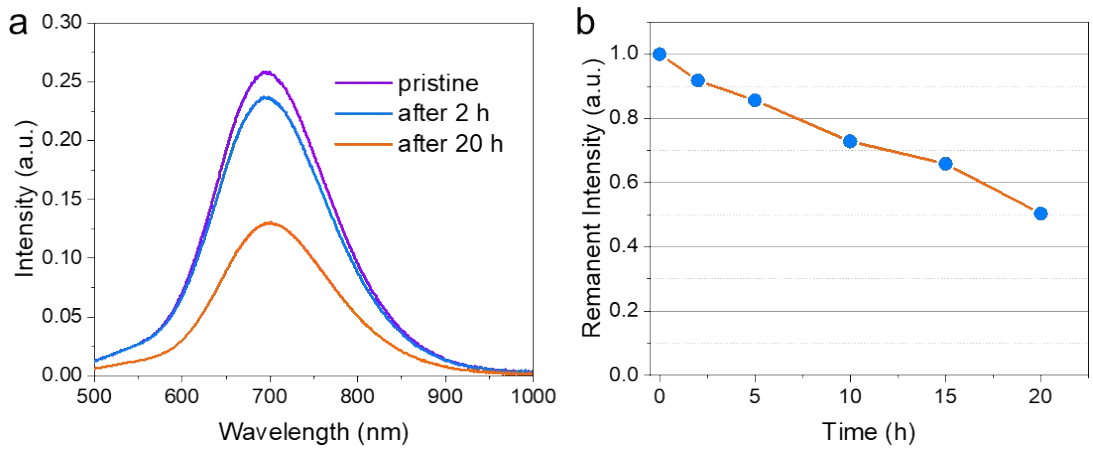

Figure S20. Stability test of NIR pc-LED with continuous operation time at 20 mA (a) EL spectra under various operation time. (b) Remanent EL intensity curve with operation time.

REFERENCES

(1) Su, B.; Li, M.; Song, E.; Xia, Z. Sb^{3+} -Doping in Cesium Zinc Halides Single Crystals Enabling High-Efficiency Near-Infrared Emission. *Adv. Funct. Mater.* **2021**, *31* (40), 2105316.

(2) Xiong, G.; Yuan, L.; Jin, Y.; Wu, H.; Qu, B.; Li, Z.; Ju, G.; Chen, L.; Yang, S.; Hu, Y. Highly Efficient and Stable Broadband Near-Infrared-Emitting Lead-Free Metal Halide Double Perovskites. *J. Mater. Chem. C* **2021**, *9* (38), 13474–13483.

(3) Cheng, X.; Li, R.; Zheng, W.; Tu, D.; Shang, X.; Gong, Z.; Xu, J.; Han, S.; Chen, X. Tailoring the Broadband Emission in All-Inorganic Lead-Free 0D In-Based Halides

through Sb^{3+} Doping. *Adv. Opt. Mater.* **2021**, *9* (12), 2100434.

(4) Lin, H.; Wei, Q.; Ke, B.; Lin, W.; Zhao, H.; Zou, B. Excitation-Wavelength-Dependent Emission Behavior in $(NH_4)_2SnCl_6$ via Sb^{3+} Dopant. *J. Phys. Chem. Lett.* **2023**, *14* (6), 1460–1469.

(5) Su, B.; Geng, S.; Xiao, Z.; Xia, Z. Highly Distorted Antimony(III) Chloride $[Sb_2Cl_8]^{2-}$ Dimers for Near-Infrared Luminescence up to 1070 nm. *Angew. Chem. Int. Ed.* **2022**, *61* (33), e202208881.

(6) Li, B.; Jin, J.; Yin, M.; Zhang, X.; Molokeev, M.; Xia, Z.; Xu, Y. Sequential and Reversible Phase Transformations in Zero-Dimensional Organic-Inorganic Hybrid Sb-Based Halides towards Multiple Emissions. *Angew. Chem. Int. Ed. 61* (49), e202212741.

(7) Morad, V.; Yakunin, S.; Benin, B. M.; Shynkarenko, Y.; Grotevent, M. J.; Shorubalko, I.; Boehme, S. C.; Kovalenko, M. V. Hybrid 0D Antimony Halides as Air-Stable Luminophores for High-Spatial-Resolution Remote Thermography. *Adv. Mater.* **2021**, *33* (9), 2007355.